Please cite the Published Version

Extracting Residence Times of Nitric Oxide on Graphene through combination of Time-of-Flight and Velocity Map Imaging

Thomas Greenwood,[a] Sven P. K. Koehler*[b]

[a] Department of Natural Sciences, Manchester Metropolitan University, Manchester M1 5GD, UK

[b] Forschungszentrum Energie - Mobilität - Prozesse, Ricklinger Stadtweg 120, Hochschule Hannover, 30459 Hannover, Germany.

[a] t.greenwood@mmu.ac.uk

[b] sven.koehler@hs-hannover.de

Abstract

In this work, energy transfer between nitric oxide radicals and graphene was measured as a function of incidence energy, and residence times of the trapped NO molecules were extracted. This was done by combining Time-of-Flight methods with Surface-Velocity Map Imaging and by forward-simulation of the expected arrival profiles. Combining these two techniques allows us to derive those residence times even though the employed molecular beams have opening times that would otherwise prevent such measurements if only one of these experimental techniques was used in isolation. We find that significant energy transfer to the graphene occurs, increasing with increasing incidence energy, and that trapped NO may reside on the graphene for tens of microseconds at room temperature.

1. Introduction

Scattering events of atoms or molecules on surfaces can broadly be divided into two mechanisms, namely 1) a direct scattering mechanism in which the incoming projectile scatters off the surface elastically or − more frequently - inelastically, and 2) a trapping-desorption mechanism in which the incoming atom or molecule may reside at the surface for some time (the residence time) before desorbing from the surface.[1] The molecule may even thermalise at the surface before desorbing, or may become permanently trapped.[2]

The residence times of the incoming projectiles at a surface have been measured using various techniques, but have probably been more successfully calculated over the past decades, as the measurement of residence times on the order of microseconds or less using (commercial) molecular beams with pulse lengths of tens or hundreds of microseconds poses a variety of challenges.[3] Two rather elegant experimental approaches to measure residence times – both by the Wodtke group – have been devised in the last few years and employed to measure accurate residence times for CO on Pt(111) and Pd(111) and are compared with the current work further on.[4,5]

We have over the last few years applied the technique of surface-velocity map imaging (S-VMI) to the photodesorption [6, 7, 8] and scattering off surfaces,[9, 10] and in the latter case realised that the velocity of the incoming and outgoing projectiles can be measured using both, the time-of-flight (TOF) as well as the VMI technique. TOF methods measure the time t to traverse a known flight path s and calculate the speed using $c = s/t$, but if collisions with a surface are involved during that flight and the molecule is trapped at the surface, the flight time t also includes contributions from the residence time, hence potentially distorting the obtained results towards slower velocities. Since VMI yields the velocity of incoming and scattered

molecules directly, the simultaneous measurement of TOF data and VM images can help to extract residence times.

The chemical system to which this S-VMI/TOF combination has been applied here is the scattering of nitric oxide, NO, off graphene supported on gold. NO was chosen as a radical which can potentially react with the graphene through its unpaired electron. It is, of course, also straightforwardly detected using resonance enhance multi-photon ionisation (REMPI) spectroscopy,[11] and we have previously studied the speed and angular distribution of NO scattered off graphene on gold,[9, 10] and performed molecular dynamics simulations on the system.[12]

Graphene, a 2-dimensional hexagonal arrangement of sp^2-hybridised carbon atoms, has gained much attention over the past 20 or so years since the discovery of its unusual physical and chemical properties.[13] Amongst these is e.g. the tunability of its band gap (pristine graphene is actually a zero band gap material) by functionalisation through chemical reactions.[14, 15] For related sum-frequency generation experiments, we have previously modified graphene in our group by attaching phenyl groups or hydrogen atoms;[16, 17] the latter has the potential as a light-weight solid hydrogen storage medium.[18] A first step towards understanding chemical reactions (leading to functionalization) on graphene are scattering studies which can reveal the fundamentals of the collision process and the potential bond-formation process on graphene.

There are only a handful of groups who have studied the scattering dynamics of projectiles off graphene, graphite or HOPG, e.g. through modelling by Hase and co-workers (N$_2$ with graph**ite**, detecting mainly single scattering events with much of the energy lost to the graph**ite** lattice), by Nieman *et al.* and Jayee *et al.* for N(^{4}S) and O(^{3}P) atoms off graphene (at

4

high collision energies relevant to the re-entry of spacecrafts), by Juaristi and co-workers (O_2 scattered off HPOG), and experimentally by Minton and co-workers (N_2 off HOPG).[19, 20, 21, 22, 23] More recently, Jackson and Beck combined quantum-mechanical calculations with elegant state-to-state scattering experiments of CH_4 on Nickel surfaces as well as Ni surfaces passivated by graphene.[24]

It may be important to note here that graphene, a single layer of carbon atoms held together by covalent bonds, is only loosely bound to the substrate (typically a metal such as e.g. copper, gold, or iridium) with distances between 3 Å and 4 Å, and hence has potential to undergo reactive collisions with the incoming projectile, though graphite and HOPG can also be throught of as a single layer of graphene attached to graphite with similar interlayer distances, and could therefore be equally susceptible to chemical reactions.

The work by Wodtke and co-workers serves as a benchmark for atomic scattering off graphene.[25] Short H-atom pulses were directed onto graphene, and a combination of experimental and theoretical analysis revealed temporary bond formation between the H atoms and graphene.

The large body of state-resolved NO scattering studies off graph**ite** from the 1980s broadly found that 1) isotropic scattering dominates at lower surface temperatures caused by trapping desorption, whereas 2) specular scattering dominates at higher temperatures.[26, 27, 28, 29, 30] At our 0° incidence angle experiments at room temperature, we find narrow angular distributions, significant energy loss,[9] and a weak trapping desorption mechanism, and since these scattering dynamics are established, though interestingly not always in agreement with the earlier graphite studies (the much narrower angular distributions from graphene is highlighted here), this paper describes the effect of incidence energy on energy transfer and

the estimation of residence times through the combination of TOF and S-VMI

measurements.

2. Experimental

The experimental set-up has been described previously,[9, 10] but is briefly summarised here,

with the most important aspects highlighted, see also Figure 1. Molecular beams with three

different velocities were prepared in these experiments by expanding 1) a 2% mixture of NO

in He, 2) a mixture of 4% NO, 20% Ar and 76% He, and 3) 4% NO with 50% Ar and 46% He, to

investigate the influence of incident energy on energy loss to the graphene lattice. The

respective molecular beam is expanded through a General Valve nozzle and skimmed via a

Beam Dynamics 0.5 mm skimmer before entering the differentially-pumped surface chamber

(base pressure of 5 x 10^{-9} Torr) housing the graphene sample supported on gold. The graphene

sample was CVD grown on copper and transferred onto gold prior to insertion into the

vacuum chamber. The NO molecules fly along the surface normal (the y dimension in Figure

1 a, downwards in the lab frame) towards the graphene surface where they are scattered

back up along the y axis, while being intersected, both on approach of the surface as well as

after being scattered, by an unfocused laser beam (Radiant Dyes NarrowScan at ~0.8 mJ per

pulse) perpendicular to the surface normal (along x in Figure 1 a) and 5.5 cm above the

graphene. We tuned the laser to around 226.9 nm to excite on the $A\ ^2\Sigma \leftarrow X\ ^2\Pi(0,0)$

transition at the bandhead of the P_2 and P_{12} branch where multiple rotational lines overlap

such that the influence of different rotational distributions before and after collision are

minimized.

The NO is ionised in a 1+1 REMPI scheme and the cations subsequently accelerated by the

VMI optics towards a MCP/Phosphor screen detector. The signal on the MCP is either

recorded as the overall signal, or alternatively the fluorescence on the phosphor screen is imaged by a triggered Net GmbH CMOS camera. The experiment as a whole is triggered at 10 Hz using an SRS DG645 delay generator. This allows for the timing to be altered between the beam opening and the laser, which can coarsely help to distinguish e.g. the initial molecular beam from the scattered beam. However, at typical molecular beam opening times of ~300 µs and round-trip times of the molecular beam from the laser intersection to the graphene surface and the scattered beam back to the laser (~11 cm) of tens of microseconds, these pure time-of-flight time measurements are error-prone, and the surface-VMI technique plays to its strength, namely by being able to distinguish the different components based on their position in the images.

3. Results and Discussion

Three separate components can be distinguished in the composite VM images as shown in Figure 1 b, namely the molecular beam itself (blue rectangle), the directly scattered NO (red) and trapping-desorbed NO in orange. We thus defined regions-of-interest (ROI) for the various components as shown and recorded time-of-flight profiles for each component
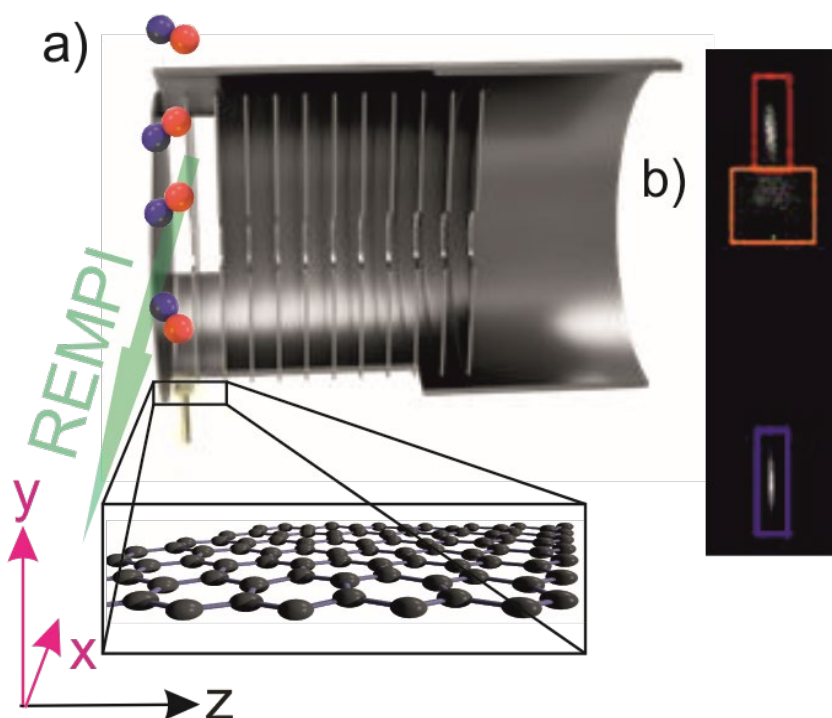

Figure 1: a) Cut through experimental set-up, the molecular beam pointing vertically down along the *y* axis towards the graphene surface in the *xz* plane, the beam and subsequently scattered NO molecules are intersected by the laser along *x*. b) Composite image of the components of NO arrival positions with their respective regions of interest. The molecular beam in blue, directly scattered NO in red and trapping desorbed NO in orange, where the green dot represents the spot of zero velocity in the *x* and *y* dimensions.

separately.

The coloured rectangles show the regions-of-interest (ROI) for each component. The signals integrated over each ROI (i.e. for the three components separately) as a function of delay time between the opening of the molecular beam and the REMPI laser are shown in Figure 2 b)-d) and are significantly more intense for the incoming molecular beam (Figure 2 b) than

for the directly scattered component (c) which is again much more intense than that of the trapping desorbed NO (d).

Figure 2 a shows the signal integrated over the entire detector region, which is not only unable to distinguish between the different components, but it can be seen that the signals due to scattering and trapping are so weak that they barely show up above the noise in the tail of the total signal.
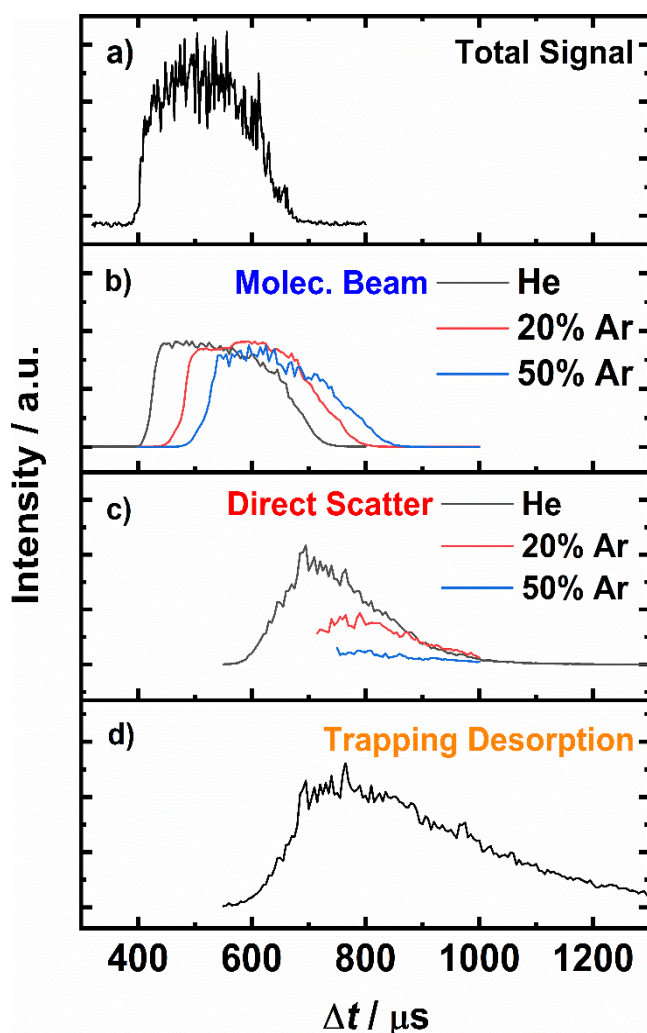
Figure 2: a) Time-of-flight scan of NO extracted directly from the overall detector signal, for a 2% NO mixture in He, consisting of all components. b) TOF scan of NO extracted from ROI relevant to the molecular beam for three NO mixtures. c) TOF scans of directly scattered NO. d) Delay scan of the trapping-desorbed NO for a pure helium mixture. Signal intensities for (a), (b), (c) and (d) not on the same intensity scale, these cannot be compared as (a) uses the integrated signal, and the ROI for (b), (c), and (d) are of different size.

It can be seen that the onset of the total signal in Figure 2 a) coincides with the onset of the molecular beam signal (b) as expected, and that the scatter and trapping-desorption (TD) components rise 200-300 µs later than the molecular beam due to the round-trip time to the graphene surface and back to the laser detection region. It should be noted that the rising edge for the two argon mixtures in Figure 2 c has been removed because for the slower beams, the ROIs are closer together, and the much more intense direct scatter quickly saturates, 'spilling' over into the ROI of the trapping desorption component. It should also be noted that the trapping desorption trace, shown in Figure 2 d, was only recorded for the pure helium mixture, but was too weak for the two slower mixtures.

The slower molecular beam velocity of the Ar-heavy mixtures can be observed in Figure 2 b, and this extends to the directly scattered NO molecules, Figure 2 c; the signal of the TP component for the Ar-heavy mixtures was too weak to be detected, Figure 2 d, and the proximity of the trapping desorption signal to the directly scattered NO impedes a meaningful separation.

It is worth noting that the trapping desorption signal is recorded only in a small region of interest above the center of the VMI zero-velocity spot of the detector and appears on similar timescales to the directly scattered signal (i.e. is not due to background NO), but the TD signal declines over a much longer timescale compared to the directly scattered signal.

While the TOF distributions contain some information about the speed of the incoming and scattered NO molecules, the velocities can of course be directly established from the VM images such as those shown in Figure 1 b.

By recording images of e.g., the molecular beam at different delay times (to capture all contributions to the molecular beam, as the velocity distribution is different at different delay

10

times while the molecular nozzle is open) and weighing them appropriately according to their intensity at a given delay time, speed distributions such as the ones in Figure 3 a for the three different beams can be derived.
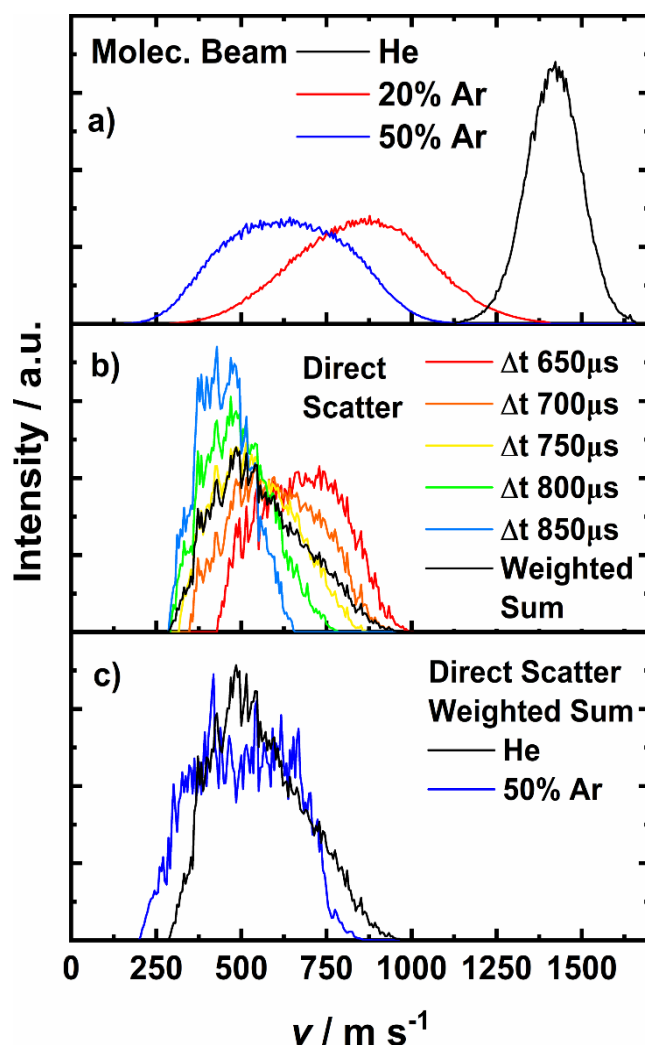

Figure 3: a) Velocity distributions of NO in the molecular beam extracted from VMI images for NO in the pure helium beam, 20% argon and 50% argon. b) Velocity distributions of directly scattered NO in the pure helium beam, where the scattered signal consists of a normalised composite image over a range of delay times between the molecular beam and the REMPI laser. c) The scattered NO velocities in the pure helium beam and 50% argon mixture over a range of delays.

Figure 3 b shows the contributions of the directly scattered NO molecules at different delay times and the weighted sum of these components. The chosen delay times become apparent when comparing with the TOF trace in Figure 2 c.

The weighted sum in black is again shown in Figure 3 c) in comparison with the same (normalised) result for the slowest (50% Ar) beam. While there is some memory of the velocity of the incoming molecular beam, much of the kinetic energy is lost in the collision
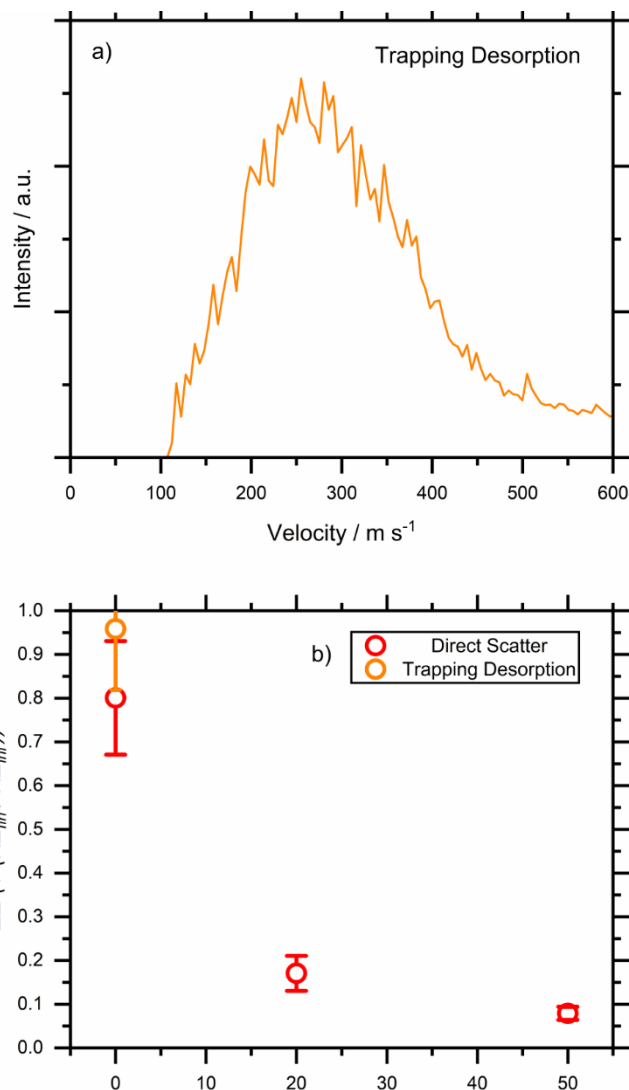
Figure 4: a) Velocity distribution of trapping-desorbed NO in a pure helium beam, extracted from VMI images. b) Reduction in energy for directly scattered and trapping desorbed NO when compared to the incoming molecular beam, for the helium beam, 20% argon and 50% argon mixtures.

process even for the directly scattered component, and this energy loss is clearly much more pronounced the faster the molecular beam. The signal of the trapping desorption component is shown for the pure He mixture in Figure 4 a, but was too weak to be recorded for the two Ar-rich mixtures.

The previously described trend that more kinetic energy is lost in the scattering process the higher the initial kinetic energy of the molecular beam is illustrated in Figure 4 b. It is feasible to assume that a high-velocity projectile impinging on the graphene is deforming the graphene lattice to a greater degree, and our previous molecular dynamics simulations indeed show ripples in the graphene after scattering. The energy transfer characteristics hence shift from strongly inelastic for high impact energies to almost elastic at low collision energies.

As previously mentioned, the simultaneous measurement of TOF profiles and VM images allows us to estimate residence times of the NO molecules on the graphene by forward convolution of the velocity profiles. In effect, this is a similar approach to those employed by the Wodtke to measure the desorption rates from surfaces either 1) by ionization of the desorbing species using two spatially and temporally separated lasers to obtain velocity information[4] or – more closely related to our approach here – by 2) recording velocity images over all relevant delay times (between the molecular beam pulse and the laser) and thus extracting kinetic information.[5]

The approach presented here, the results of which are show in Figure 5, relies on a forward convolution. This was done by simulating the overall TOF profile in a Monte Carlo fashion from the information obtained by the VM images. In brief, we obtain velocity information both 1) through the recorded TOF profiles AND 2) from the VM images. We use the velocity distribution from the images (which we consider the true velocity information) to simulate TOF profiles. These simulated TOF profiles, which do NOT include contributions from residence times, are then compared to the measured TOF profiles which DO include contributions from potential residence times. The difference between the MC-simulated

(true) TOF profiles and the (possibly delayed due to the residence time) measured TOF profiles accounts for the residence time. Moreover, VM images and measured TOF profiles can be recorded separately for the direct and the trapping-desorption component such that residence times can independently be extracted for the direct component (where residence times close to zero are expected) and the trapping-desorption component. In more detail: the velocity distribution of the initial (downward) molecular beam is know from the VM images with high precision (see Figure 2 b). As we also know the distance between the molecular beam and 1) the laser beam as well as 2) the graphene surface, and also the opening time of the molecular beam, TOF profiles of the molecular beam can be modelled based purely on the VMI data, see Figure 5 a) in grey.

Also knowing both 1) the velocity of the directly scattered component and 2) velocity of the trapping desorption component from the VM images, we can similarly simulate the TOF profiles of the returning NO molecules. The sum of the simulated TOF profiles of the downward going molecular beam and the (directly or TD) scattered molecules can be compared to the recorded TOF profiles for each ROI, see Figure 5 b) and c). While the simulated and measured TOF profiles overlap well for the direct scattering component in Fig. 5 b), the comparison of the measured and simulated trapping desorption TOF profiles differ as seen in Fig. 5 c). At longer delay times, the experimental TOF profile decays tens or hundreds of microseconds later than the simulated TOF profile, see the blue arrow in Figure 5 c). This is likely due to the residence times during which some NO molecules are trapped at the surface, and which is not accounted for in the simulations based on the VM images. The differences between the simulated and the measured TOF profiles are hence attributed to these residence times. Since trapping for individual molecules can range from a few collisions with the surface to tens or hundreds of collisions with the surface, the residence times

14

naturally span a wide range, but can with some confidence be estimated to be in the range of tens or (low) hundreds of microseconds at room temperature and at the conditions in these experiments.
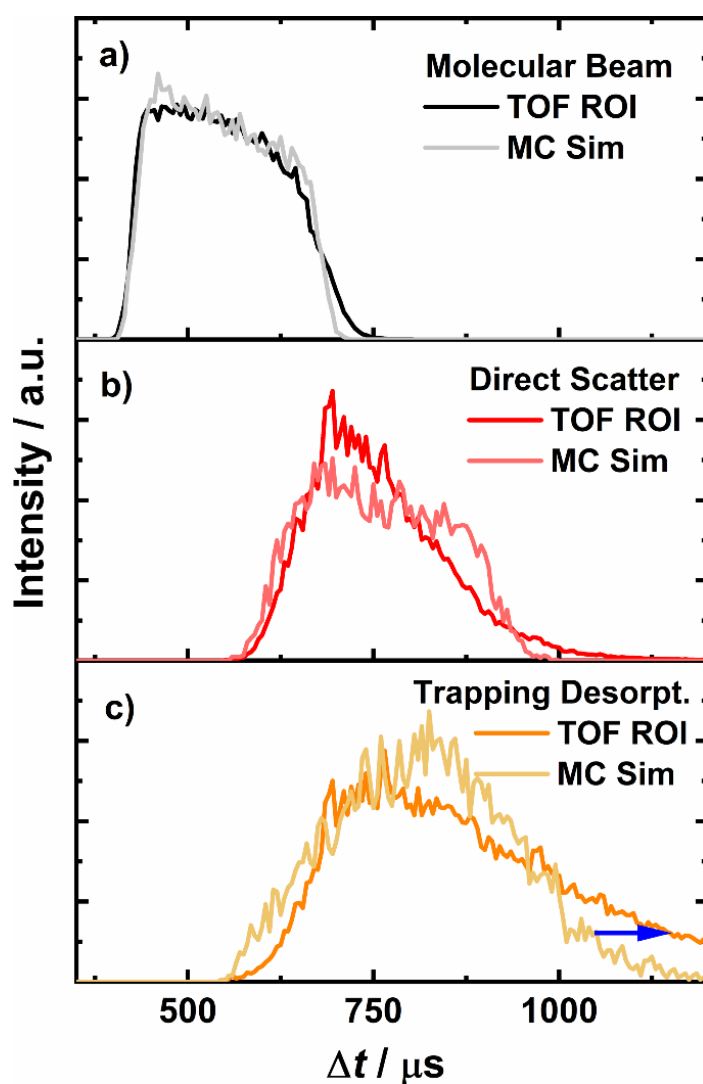

Figure 5 - Comparison of the time-of-flight profiles recorded within the regions-of-interest (black, red, orange) with the Monte Carlo simulated TOF profiles using the VM images (faded lines) for a) the molecular beam, b) the directly scattered nitric oxide molecules, and c) the trapping desorption component.

Changing the conditions, especially the surface temperature, would allow us to extract more detailed desorption kinetics, but this is not possible at present, and as such the parallel use of VMI and TOF techniques is meant to illustrate the capacity of this approach of measuring residence times.

4. Conclusions

A molecular beam of nitric oxide in helium was scattered off a graphene surface supported on gold, where the ratio of helium and argon in the beam were varied yielding three distinct mixtures and thus, incoming velocities. The nitric oxide was ionised and the two observed components, namely 1) directly scattered NO and 2) trapping desorbed NO, were probed using the surface-velocity map imaging set-up, where velocity and time of flight distributions for the two components were recorded for each beam mixture.

In the case of the directly scattered NO, as the proportion of argon in the beam increased and the incoming velocity of the nitric oxide decreased, the proportion of energy lost to the surface decreased. The proportion of energy lost during the scattering process was 0.80±0.13, 0.17±0.04 and 0.07±0.02 for the pure helium, 20% argon and 50% argon, respectively. In the case of the pure helium, the trapping desorbed NO was shown to have lost almost all (0.96±0.14) of its initial energy while for the Ar rich mixtures, the signal for the trapping desorption component was too weak for analysis.

In the case of the pure helium mixture, time of flight profiles of all three components of nitric oxide (including the molecular beam) were recorded using the appropriate regions of interest and compared against Monte-Carlo simulated distributions resulting from the velocity distributions taken from the VM images. It is clear from these comparisons that the trapping desorbed nitric oxide resides on the graphene surface on the order of the tens to low hundreds of microseconds.

While the NO molecules lose increasing amounts of their kinetic energy to the graphene surface as the incoming velocity increases, it is interesting to note that the energy lost to the surface as a proportion of the incoming velocity actually decreases with slower molecular

beams, i.e. faster beams lose more of their energy to the surface not just in total but proportionally, too. It has also been demonstrated that time of flight traces and velocity distributions taken from velocity map images can be used to estimate residence times, even in this case where the molecular beam has quite a long opening time. This estimation of residence times on the order of tens to hundreds of microseconds provides experimental supporting evidence for the trapping pathways described in our previously described MD simulations. Though due to the vastly different timescales (the simulations only lasted 4-8 ps), quantitative comparisons cannot be drawn.

It is clear from these results that further studies are required to investigate these residence times. Further experiments employing a wider range of molecular beam velocities with shorter opening times and different surface temperatures are planned.

Acknowledgements

References

[1] M. P. D'Evelyn, R. J. Madix; Reactive scattering from solid surfaces, *Surf. Sci. Rep.*, 1984, **3**, 413.

[2] J. A. Barker, D. J. Auerbach; Gas—surface interactions and dynamics; Thermal energy atomic and molecular beam studies, *Surf. Sci. Rep.*, 1985, **4**, 1.

[3] D. J. Auerbach, J. C. Tully, A. M. Wodtke; Chemical dynamics from the gas-phase to surfaces , *Nat. Sci.*, 2021, **1**, e10005.

[4] K. Golibrzuch, P. R. Shirhatti, J. Geweke, J. Werdecker, A. Kandratsenka, D. J. Auerbach, A. M. Wodtke, C. Bartels; CO Desorption from a Catalytic Surface: Elucidation of the Role of Steps by Velocity-Selected Residence Time Measurements, *J. Am. Chem. Soc.*, 2015, **137**, 1465.

[5] D. J. Harding, J. Neugebohren, H. Hahn, D. J. Auerbach, T. N. Kitsopoulos, A. M. Wodtke; Ion and velocity map imaging for surface dynamics and kinetics, *J. Chem. Phys.*, 2017, **147**, 013939.

[6] S. Abujarada, H. AlSalem, U. Chohan, G. Draper, S. Koehler; Photodesorption of nitric oxide from Au(100) using 3-dimensional surface-velocity map imaging, *J. Chem. Phys.*, 2016, **145**, 184201.

[7] S. Abujarada, C. Flathmann, S. Koehler; Translational and Rotational Energy Distributions of NO Photodesorbed from Au(100), *J. Phys. Chem. C*, 2017, **121**, 19922–19929.

[8] S. Abujarada, A. Walton, A. Thomas, U. Chohan, S. Koehler; Adsorption Site, Orientation and Alignment of NO Adsorbed on Au(100) using 3D-Velocity Map Imaging, X-ray Photoelectron Spectroscopy and Density Functional Theory, *Phys. Chem. Chem. Phys.,* 2019, **21**, 10939—10946.

[9] T. Greenwood, S. P. K. Koehler; Nitric Oxide Scattering off Graphene Using Surface-Velocity Map Imaging, *J. Phys. Chem. C,* 2021, **125**, 17853.

[10] T. Greenwood, H. S. AlSalem, S. P. K. Koehler; Velocity-Selected Rotational State Distributions of Nitric Oxide Scattered off Graphene Revealed by Surface-Velocity Map Imaging, *J. Phys. Chem.*, 2023, **127**, 1124.

[11] M. Hippler, J. Pfab; Detection and probing of nitric oxide (NO) by two-colour laser photoionisation (REMPI) spectroscopy on the A $\leftarrow$ X transition, *Chem. Phys. Lett.*, 1995, **243**, 500.

[12] T. Greenwood, S. P. K. Koehler; Molecular Dynamics Simulations of Nitric Oxide Scattering Off Graphene*, Chem. Phys. Chem*., 2022, **23**, e202200216.

[13] K. S. Novoselov, V. I. Fal'ko, L. Colombo, P. R. Gellert, M. G. Schwab, K. Kim; A roadmap for graphene, *Nature*, 2012, **490**, 192.

[14] C. Xu, P. A. Brown, J. Lu, K. L. Shuford; Electronic Properties of Halogen-Adsorbed Graphene, *Phys. Chem. C,* 2015, **119**, 17271.

[15] J. M. Englert, C. Dotzer, G. Yang, M. Schmid, C. Papp, J. M. Gottfried, H.-P. Steinrück, E. Spiecker, F. Hauke, A. Hirsch; Covalent bulk functionalization of graphene, *Nat. Chem.*, 2011, **3**, 279.

[16] H. S. AlSalem, C. Holroyd, M. Danial Iswan, A. B. Horn, M. A. Denecke, S. P. K. Koehler; Characterisation, coverage, and orientation of functionalised graphene using sum-frequency generation spectroscopy, *Phys. Chem. Chem. Phys.*, 2018, **20**, 8962.

[17] H. S. AlSalem, X. Just-Baringo, I. Larrosa, U. Monteverde, X. Jiang, Y. Feng, S. P. K. Koehler; Evidence for Site-Specific Reversible Hydrogen Adsorption on Graphene by Sum-Frequency Generation Spectroscopy and Density Functional Theory, *J. Phys. Chem. C*, 2019, **123**, 25883

[18] V. Jain, B. Kandasubramanian; Functionalized graphene materials for hydrogen storage, *J. Mater. Sci.*, 2020, **55**, 1865.

[19] M. Majumder, H. N. Bhandari, S. Pratihar, W. L. Hase; Chemical Dynamics Simulation of Low Energy N_2 Collisions with Graphite, *J. Phys. Chem. C*, 2018, **122**, 612.

[20] R. Nieman, R. Spezia, B. Jayee, T. Minton, W. Hase, H. Guo; Exploring reactivity and product formation in $N(^4S)$ collisions with pristine and defected graphene with direct dynamics simulations, *J. Chem. Phys.*, 2020, **153**, 184702.

[21] B. Jayee, R. Nieman, T. Minton, W. Hase, H. Guo; Direct Dynamics Simulations of Hyperthermal $O(^3P)$ Collisions with Pristine, Defected, Oxygenated, and Nitridated Graphene Surfaces, *J. Phys. Chem. C,* 2021, **125**, 9795–9808.

[22] A. R. Santamaría, M. Alducin, R. D. Muiño, J. I. Juaristi; Ab Initio Molecular Dynamics Study of Alignment-Resolved O_2 Scattering from Highly Oriented Pyrolytic Graphite, *J. Phys. Chem. C*, 2019, **123**, 31094.

[23] N. Mehta, V. Murray, C. Xu, D. Levin, T. Minton; Nonreactive Scattering of N_2 from Layered Graphene Using Molecular Beam Experiments and Molecular Dynamics, *J. Phys. Chem. C*, 2018, **122**, 9859–9874.

[24] J. Werdecker, B.-J. Chen, M. E. Van Reijzen, A. Farjamnia, B. Jackson, R. D. Beck; State-to-state methane-surface scattering as a probe of catalytic activity, *Phys. Rev. Res.*, 2020, **2**, 043251.

[25] H. Jiang, M. Kammler, F. Ding, Y. Dorenkamp, F. Manby, A. Wodtke, T. Miller, A. Kandratsenka, O. Bünermann; Imaging covalent bond formation by H atom scattering from graphene, *Science*, 2019, **364**, 379–382

[26] M. C. Lin, G. Ertl; Laser Probing of Molecules Desorbing and Scattering from Solid Surfaces, *Ann. Rev. Phys. Chem.,* 1986, **37**, 587-615.

[27] F. Frenkel, J. Häger, W. Krieger, H. Walther, G. Ertl, J. Segner, W. Vielhaber; Rotational state populations and angular distributions on surface scattered molecules: No on graphite, *Chem. Phys. Lett.*, 1982, **90**, 225.

[28] J. Häger, Y. R. Shen, H. Walther; State-selective velocity and angular distributions of NO molecules scattered from a graphite surface, *Phys. Rev. A*, 1985, **31**, 1962.

[29] J. Häger, H. Walther; Laser investigation of the dynamics of molecule–surface interaction: Rotational and translational energy of scattered molecules, *J. Vac. Sci. Technol. B*, 1985, **3**, 1490-1497.
[30] G. Nyman, L. Holmlid, J. B. C. Pettersson; Surface scattering of NO from graphite: A statistical description of energy distributions, *J. Chem. Phys.*, 1990, **93**, 845.

TOC Graphic